A Dual-Mode Near-Infrared Optical and Photoacoustic Imaging Agent Based on a Low Energy Absorbing Ytterbium Complex

Anton Kovalenko, Svetlana V. Eliseeva, Guillaume Collet, Saïda El Abdellaoui, Sharuja Natkunarajah, Stéphanie Lerondel, Laure Guénée, Céline Besnard, Stéphane Petoud

A Dual-mode Near-infrared Optical and Photoacoustic Imaging Agent Based on a Low Energy Absorbing Ytterbium Complex

Anton Kovalenko,[†] Svetlana V. Eliseeva,[*,†] Guillaume Collet,[†,╤] Saïda El Abdellaoui,[†] Sharuja Natkunarajah,[§] Stéphanie Lerondel,[§] Laure Guénée,[⊥] Céline Besnard[⊥] and Stéphane Petoud[*,†]

† Centre de Biophysique Moléculaire, CNRS UPR4301, Université d'Orléans, Rue Charles Sadron, 45071 Orléans Cedex 2, France

§ TAAM imagerie in vivo, CNRS UAR44, 3B rue de la Férollerie, 45071 Orléans Cedex 2, France

╤ Le Studium Loire Valley Institute for Advanced Studies, Orléans & Tours, France

⊥ Laboratory of Crystallography, University of Geneva, Quai Ernest Ansermet 24, 1211 Geneva 4, Switzerland

Supporting Information Placeholder

ABSTRACT: Near-infrared (NIR) luminescence and photoacoustic (PA) imaging have attracted an increasing attention for the real-time monitoring of biological samples due to high sensitivity, resolution and pronounced signal detection depth, respectively. For improved contrast, both techniques require imaging agents possessing high absorption in the red-NIR range. Herein, we took advantage of a ternary complex formed with the anionic ytterbium(III) *tetrakis*(2-thenoyltrifluoroacetonate) ($[Yb(tta)_4]^-$) and the cationic NIR-absorbing chromophore, 1,1′-diethyl-2,2′-dicarbocyanine (Cy^+) to evaluate its potential to act as a dual-mode NIR luminescence and PA imaging agent. We demonstrated that, upon excitation with red-NIR light, $Cy[Yb(tta)_4]$ encapsulated into polystyrene nanoparticles is able to generate both NIR Yb^{3+} emission and PA signal in an imaging experiment performed in a tissue-mimicking phantom.

The field of molecular imaging and medical diagnosis has witnessed an exponential growth in the last few years, largely due to the rapid development of non-invasive, real-time, easy to use, portable and convenient for patient imaging modalities. Among them, near-infrared (NIR) luminescence[1-3] and photoacoustic (PA) imaging[4-7] use non-ionizing excitation followed by the detection of emission signals or acoustic waves, respectively. NIR luminescence imaging is a very sensitive technique that allows molecular visualizations with high resolution (<10 μm) and contrast at depths of few mm. [2-3, 8] Due to different absorption of light by biological molecules (hemoglobin, lipids, collagen, water), PA imaging, depending on the configuration and the frequency of the ultrasound detector that is used, can offer anatomic and functional information in addition to molecular imaging at depths up to 6 cm.[9-11]

To enhance contrast both NIR luminescence and PA imaging modalities require the use of imaging agents possessing specific properties, a common one being a high absorbance in the biological transparency window (650–1700 nm).[1-2, 12] Since acoustic waves are much less attenuated by biological molecules than light, dual-mode NIR luminescence and PA imaging agents will allow to collect images at greater depths and complement optical performance by absorption contrast information, e.g. tissue vascularization and oxygenation, or lipids concentration, therefore, broadening the scope of the detection and diagnostic. In respect to biology, a single imaging agent implies a unique characterization of its behavior (biodistribution, toxicity and kinetics). As of today the number of such dual-mode imaging probes remains scarce[13-18] despite the increasing demand.[19]

Lanthanide(III)-based probes have shown to be promising candidates for NIR luminescence imaging[20-22] because of their unique optical properties[23] resulting from the forbidden nature of most of f-f transitions, such as line-like emission bands in the visible and in the NIR domains with fixed barycenter positions and excellent photostability.[24-25] However, free lanthanide(III) cations (Ln^{3+}) have very low absorption cross-sections. To generate a sufficient number of photons using ordinary excitation sources, they need to be sensitized with a highly absorbing chromophore which can absorb the excitation light and transfer the resulting energy to the electronic levels of Ln^{3+}, leading to their characteristic emission. This process is called the "antenna effect".[26-27]

Luminescent Ln^{3+} β-diketonates[28] have been used for biological applications due to the ease of synthesis and the versatility of the chemistry of the β-diketones.[29] However, except few examples,[30-34] the majority of luminescent Ln^{3+} β-diketonates can only be sensitized by UV- or blue-absorbing chromophores.[23, 29, 35] In general, the creation of biologically compatible NIR-absorbing-NIR-emitting (NIR-NIR) Ln^{3+} complexes remains a challenge.[30-31] A few examples are based on Ln^{3+} tetrapyrrole and Kläui ligands,[36] while the most relevant one is Er^{3+} bacteriochlorin.[37] Such complexes usually require multi-step syntheses and Q bands at wavelengths above 600 nm exhibit low absorptivity ($\varepsilon < 10^4$ $M^{-1}cm^{-1}$). We have therefore designed, synthesized and characterized a *tetrakis* β-diketonate $Cy[Yb(tta)_4]$ (Figure 1) containing a NIR-emitting Yb^{3+}, a NIR-absorbing cationic chromophore 1,1′-diethyl-2,2′-dicarbocyanine (Cy^+) with a large molar absorption

coefficient ($\varepsilon_{710\ nm}$ ~$2.5\cdot10^5$ $M^{-1}cm^{-1}$) and four 2-thenoyltrifluoroacetonate (tta^-) ligands. To ensure stability in aqueous solution and allow NIR and PA imaging experiments using specially-designed phantoms mimicking blood vessels and biological tissues, $Cy[Yb(tta)_4]$ has been encapsulated inside 100-nm NH_2-functionalized polystyrene (PS/NH_2) nanoparticles (NPs). The resulting $Cy[Yb(tta)_4]$_α@PS/NH_2 NPs (α is the loading concentration, *vide infra* and Supporting Information) have been used in a proof-of-concept demonstration of their ability to, upon NIR excitation, emit NIR light and generate PA signal.

$Cy[Yb(tta)_4]$ was synthesized in a one-step reaction using an adapted literature procedure[38] from Cy iodide, Htta and $Yb(NO_3)_3{\cdot}5H_2O$ in EtOH-H_2O (Scheme S1). Its composition was confirmed by elemental analysis, PXRD and FTIR spectroscopy (Supporting Information). A single crystal of $(Cy[Yb(tta)_4])_3(CH_3CN)_4(Et_2O)_2$ was obtained by diffusion of Et_2O vapors into an acetonitrile saturated solution of $Cy[Yb(tta)_4]$. Crystallographic analysis (Figure 1) has revealed that it is constituted by Cy^+ and $[Yb(tta)_4]^-$, with the shortest distance between Cy^+ and Yb^{3+} being ~7.3 Å. Yb^{3+} is coordinated by eight oxygen atoms belonging to four tta^- ligands and adopts a distorted square antiprismatic coordination environment (Figure S1). No solvent molecule is directly coordinated to Yb^{3+}.

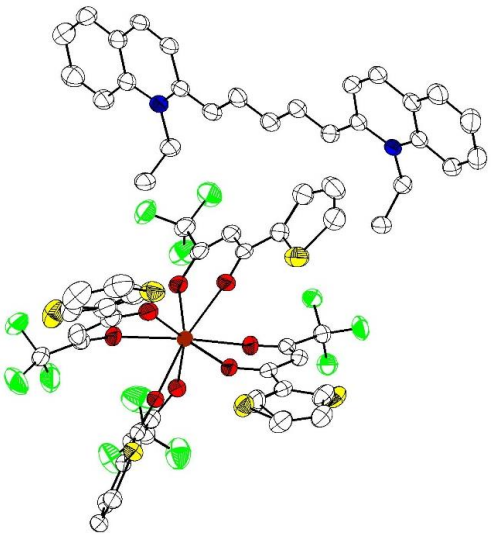

Figure 1. Molecular structure of $(Cy[Yb(tta)_4])_3(CH_3CN)_4(Et_2O)_2$ obtained from X-ray diffraction on a single crystal. Thermal ellipsoids are drawn at 50% probability (Ortep view). Hydrogen atoms and lattice solvent molecules are omitted for clarity. Colour code: C, white; O, red, N, blue, S, yellow, F, green; Yb, brown.

The photophysical properties of $Cy[Yb(tta)_4]$ have been studied in DMF solution. The absorption spectrum (Figure 2, dashed trace, Figure S5) of $Cy[Yb(tta)_4]$ presents a broad band in the red-NIR spectral range (550-780 nm; ε_{715nm}= $2.16\cdot10^5$ $M^{-1}cm^{-1}$) that can be assigned to $\pi\rightarrow\pi^*$ transitions of the Cy^+ chromophore.[39-40] Under excitation at 660 or 715 nm, $Cy[Yb(tta)_4]$ exhibits the characteristic Yb^{3+} emission signal centered at 980 nm assigned to the $^2F_{5/2}\rightarrow{}^2F_{7/2}$ transition (Figure 2, Figure S7). As Yb^{3+} and tta^- do not possess any electronic transitions in the range of 500–800 nm, the only possibility to populate the excited states of Yb^{3+} is by using the electronic structure of Cy^+, generating this way an "antenna effect".[26] An evaluation of the resistance to photobleaching was performed in solution by comparing, upon constant illumination at 660 nm, the intensity of the Yb^{3+} signal arising from $Cy[Yb(tta)_4]$ with the broad-band signal of the free Cy iodide that possess an apparent maximum of emission at 750 nm. A lower decrease of the emission signal is observed for $Cy[Yb(tta)_4]$ as a strong indication of a higher photostability (Figure S9). Experimental luminescence decay curves upon monitoring the emission of Yb^{3+} at 980 nm have been best fitted with a mono-exponential function (τ_{obs} = 8.2±0.7 μs) confirming the presence of only one type of Yb^{3+}-emitting species in the DMF solution of $Cy[Yb(tta)_4]$ and being in agreement with the molecular structure (Figure 1). Mono-exponential luminescence decays were also observed in CH_3OH and CD_3OD solutions of $Cy[Yb(tta)_4]$. The obtained values of τ_{obs} (1.4±0.1 μs and 18.5±0.1 μs, respectively) allowed to estimate the Yb^{3+} hydration number q which was found to be one (Table S4).[41] Quantum yields (Q_{Yb}^{Cy}) were measured in DMF solution to evaluate the global efficiency of the Yb^{3+} sensitization upon Cy^+ excitation at 660 nm. The obtained value of $(3.5\pm0.4)\cdot10^{-4}$ is high in comparison to the quantum yields of the few examples of NIR-NIR coordination compounds such as Yb^{3+} MOF ($9.0\cdot10^{-5}$, λ_{ex} = 660 nm, in solid)[34] or Er^{3+} bacteriochlorin complex ($1.38\cdot10^{-4}$, λ_{ex} = 760 nm, in CH_2Cl_2).[37]

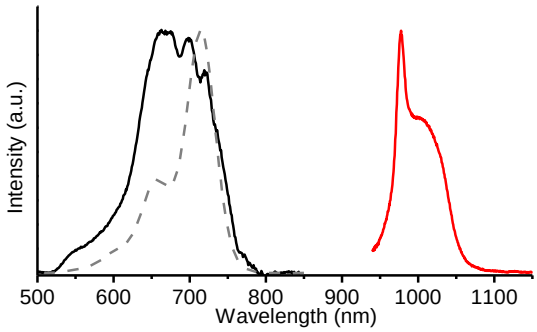

Figure 2. Corrected and normalized (left – solid black traces) excitation spectra (λ_{em} = 980 nm) and (right – solid red traces) emission spectra (λ_{ex} = 660 nm) of $Cy[Yb(tta)_4]$ (14 μM in DMF) at room temperature. Normalized absorption spectrum is superimposed for comparison (dashed grey traces).

To evaluate the potential of $Cy[Yb(tta)_4]$ for NIR and PA imaging and to overcome its limited solubility in water, we loaded it inside 100 nm polystyrene NPs coated with NH_2 groups (PS/NH_2) using a swelling methodology (Supporting Information).[42] Aqueous suspensions of colored $Cy[Yb(tta)_4]$_α@PS/NH_2 NPs with different loading concentrations α (0.54–108 nmol/mg, Table S5) were obtained. For comparison, we also prepared aqueous suspensions of Cy iodide incorporated NPs (Cy iodide_β@PS/NH_2) with different loading concentrations β (0.37–76 nmol/mg, Table S6).

Upon excitation at 660 or 750 nm into the $\pi\rightarrow\pi^*$ bands located on the Cy^+ chromophore (Figure S22), aqueous suspensions of $Cy[Yb(tta)_4]$_α@PS/NH_2 NPs with α≥30 nmol/mg exhibit NIR Yb^{3+} emission (Figures S25). Moreover, excitation spectra are similar to the ones acquired for the free $Cy[Yb(tta)_4]$ complex in DMF and match the shapes of the absorption ones. These observations show that the incorporation of the Yb^{3+} complex in the PS/NH_2 NPs doesn't affect its spectral properties and that the antenna effect is maintained.

Quantitative photophysical data were also collected for Cy[Yb(tta)$_4$]_α@PS/NH$_2$ NPs with the highest loading concentration α (108 nmol/mg). Luminescence decay curves obtained upon monitoring the emission at 980 nm were best fitted with a bi-exponential function, indicating the presence of Yb^{3+} in two different coordination environments. The longest τ_{obs} (2.5±0.6 µs) can be associated with Yb^{3+} located in the core of the NPs. The shortest value of τ_{obs} (0.35±0.05 µs) corresponds toYb^{3+} located closer to the surface, being therefore more exposed to sources of non-radiative deactivations.[42-43] The measured Q_{Yb}^{Cy} value of (3.8±0.4)·10^{-6} is the first example of an absolute quantum yield for a water-compatible system based on a NIR-NIR Yb^{3+} complex formed with an organic ligand.

A significant decrease of the Q_{Yb}^{Cy} was observed for Cy[Yb(tta)$_4$] when loaded inside of NPs and measured in water. This behavior can be attributed to a non-radiative quenching of Yb^{3+} through the overtones of O–H vibrations of the water molecules that is also reflected by the shortening of Yb^{3+} τ_{obs} values.

PA properties of aqueous suspensions of Cy[Yb(tta)$_4$]_α@PS/NH$_2$ and Cy iodide_β@PS/NH$_2$ NPs were investigated using blood vessels mimicking polymer tubes inserted into a custom-made phantom filled with water[44] (Figure S29). PA spectra profiles of both types of NPs, Cy[Yb(tta)$_4$]_α@PS/NH$_2$ (Figure 3a, solid traces) and Cy iodide_β@PS/NH$_2$ (Figure S30), are similar to those of the corresponding absorption spectra[17, 45-48] (Figure 3a, dashed traces; Figures S22-23). Quantitative data were obtained by measuring the PA signal intensity at its maximum (λ_{ex} = 720 nm). The analysis of these results reveals that the PA signal intensity depends linearly (i) on the amount of molecules loaded in NPs, α or β (Figure 3b), and (ii) on the concentration of NPs in suspension[45] (Figure S31). For a comparable amount of chromophores per NP, Cy[Yb(tta)$_4$]_α@PS/NH$_2$ generates a twice more intense PA signal in comparison to Cy iodide_β@PS/NH$_2$ NPs (Figure 3b, Figure S32). This enhancement is attributed to the difference between the absorption spectra of Cy[Yb(tta)$_4$]_α@PS/NH$_2$ and Cy iodide_β@PS/NH$_2$ NPs (Figures S22-23). Moreover, for a similar chromophore concentration, Cy[Yb(tta)$_4$]_α@PS/NH$_2$ NPs show a PA signal that is as intense as the one recorded for the indocyanine green (Figure S32), an FDA approved molecule which is considered to be a gold standard for *in vivo* PA imaging.[49]

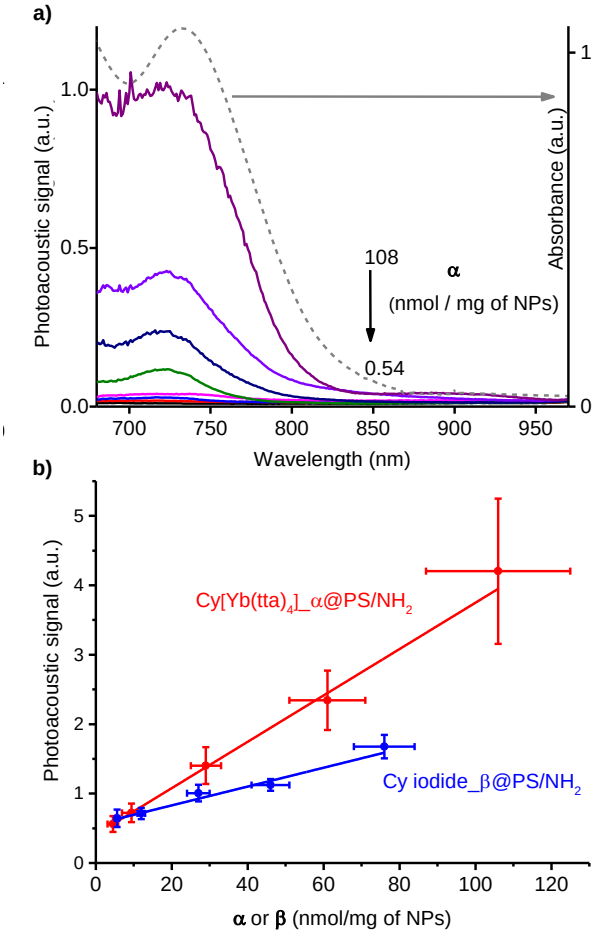

Figure 3. (a) PA spectra (left scale, solid traces, α = 0.54–108 nmol/mg) and the corresponding absorption spectrum (right scale, dashed trace, α = 62 nmol/mg) of Cy[Yb(tta)$_4$]_α@PS/NH$_2$ NPs. (b) Dependence of the PA signal recorded upon excitation at 720 nm on α (Cy[Yb(tta)$_4$]_α@PS/NH$_2$, red line, R^2 = 0.995) or β (Cy iodide_β@PS/NH$_2$, blue line, R^2 = 0.96). All data for 10 mg/mL aqueous suspensions of NPs.

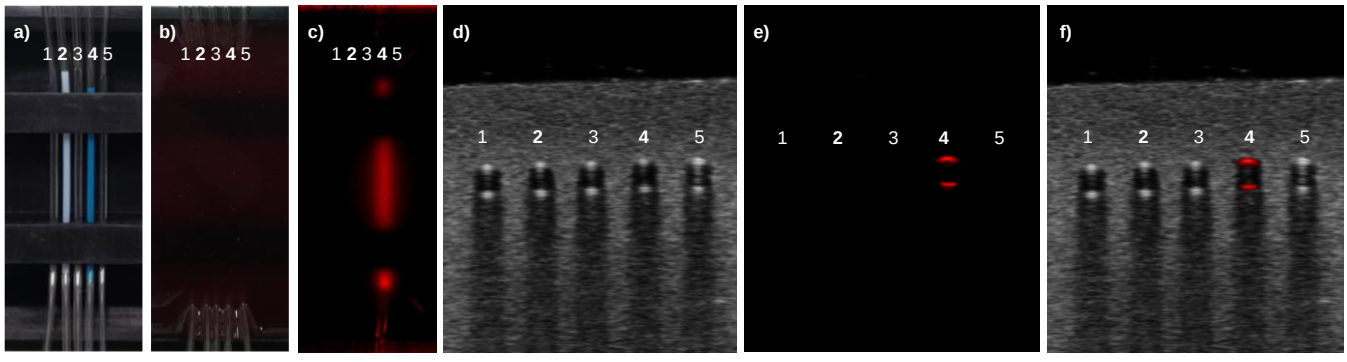

Figure 4. Color images of blood vessels mimicking polymer tubes filled with (1, 3, 5) water or 10 mg/mL aqueous suspensions of (2) PS/NH$_2$ and (4) Cy[Yb(tta)$_4$]_α@PS/NH$_2$ (α = 108 nmol/mg) NPs, and inserted into a custom-made phantom (a) without media and (b) filled with tissue-mimicking media (thickness of the top layer is 3 mm). (c) NIR luminescence image upon laser excitation at 637 nm. Yb^{3+} signal was detected with a 996 nm band-pass 70 nm filter, τ_{exp} = 2 ms. (d) Ultrasound, (e) PA and (f) merge of (d) and (e) images; λ_{ex} = 720 nm.

To further evaluate the potential of Cy[Yb(tta)$_4$]_α@PS/NH$_2$ (α = 108 nmol/mg) NPs as imaging agents, NIR luminescence and PA images were acquired using a custom-designed phantom filled with tissue-mimicking media and containing blood vessels mimicking polymer tubes (Figure 4, Figure S33). NIR Yb^{3+} luminescence, although scattered, was unambiguously detected through a 3 mm layer of a tissue-mimicking media. In addition, sharp PA signal arising from the tube filled with an aqueous suspension of Cy[Yb(tta)$_4$]_α@PS/NH$_2$ NPs was clearly distinguished by superposition of ultrasound and PA images obtained upon excitation at 720 nm.

In summary, we have created NIR-NIR Yb^{3+} complex that can operate as a dual-mode NIR luminescence and PA imaging agent. We took advantage of Cy[Yb(tta)$_4$] that contains Yb^{3+} *tetrakis*(2-thenoyltrifluoroacetonate) and a cyanine chromophore with large molar absorptivity at low energies. When excited with red-NIR light, Cy[Yb(tta)$_4$] in solution demonstrates the highest Ln^{3+} quantum yield among NIR-NIR Ln^{3+} complexes reported to date.[34, 37] Moreover, Yb^{3+} NIR luminescence and PA signals arising from aqueous suspensions of PS/NH$_2$ NPs loaded with Cy[Yb(tta)$_4$] could be unambiguously detected through a 3 mm of a tissue-mimicking phantom under excitation with red-NIR light. These results show great promises for the creation of a new generation of imaging agents based on Cy[Yb(tta)$_4$]@ PS/NH$_2$ NPs, while the quantification of the Yb^{3+} emission in the NIR is the first example of an absolute quantum yield for the NIR-NIR water-compatible system based on Yb^{3+} complex. Remaining a proof-of-concept work, we believe that the same strategy, due to its versatility, can be extended to other NIR luminescence and/or PA imaging agents based on NIR-NIR Ln^{3+} coordination compounds towards practical applications.

ASSOCIATED CONTENT

Supporting Information

The Supporting Information is available free of charge on the ACS Publications website.

Experimental details and additional information about the synthesis and characterization of Cy[Ln(tta)$_4$], Cy[Yb(tta)$_4$]_α@PS/NH$_2$ and Cy iodide_β@PS/NH$_2$, including absorption spectroscopy, dynamic light scattering, inductively coupled plasma atomic emission spectroscopy, Fourier-transform infrared spectroscopy, single crystal and powder X-ray diffraction, photoluminescence spectroscopy, NIR luminescence and PA imaging data (PDF).

Crystal structure of $(Cy[Yb(tta)_4])_3(CH_3CN)_4(Et_2O)_2$. CCDC 2172491 contains the supplementary crystallographic data for this paper. The data can be obtained free of charge from The Cambridge Crystallographic Data Centre via www.ccdc.cam.ac.uk/structures.

Printable file for the custom-made 3D printed phantom (Phantome_insert and Phantome_support.123dx).

AUTHOR INFORMATION

Corresponding Authors

Svetlana V. Eliseeva – Centre de Biophysique Moléculaire, CNRS UPR4301, Université d'Orléans, Rue Charles Sadron, 45071 Orléans, Cedex 2, France; orcid.org/0000-0002-1768-8513; Email: svetlana.eliseeva@cnrs-orleans.fr

Stéphane Petoud – Centre de Biophysique Moléculaire, CNRS UPR4301, Université d'Orléans, Rue Charles Sadron, 45071 Orléans, Cedex 2, France; orcid.org/0000-0003-4659-4505; Email: stephane.petoud@inserm.fr

Authors

Anton Kovalenko – Centre de Biophysique Moléculaire, CNRS UPR4301, Université d'Orléans, Rue Charles Sadron, 45071 Orléans, Cedex 2, France; orcid.org/0000-0003-2417-2846;

Guillaume Collet – Centre de Biophysique Moléculaire, CNRS UPR4301, Université d'Orléans, Rue Charles Sadron, 45071 Orléans, Cedex 2, France; Le Studium Loire Valley Institute for Advanced Studies, Orléans & Tours, France; orcid.org/0000-0002-0355-563X;

Saïda El Abdellaoui – Centre de Biophysique Moléculaire, CNRS UPR4301, Université d'Orléans, Rue Charles Sadron, 45071 Orléans, Cedex 2, France; orcid.org/0000-0001-9286-0603;

Sharuja Natkunarajah – TAAM imagerie in vivo, CNRS UAR44, 3B rue de la Férollerie, 45071 Orléans Cedex 2, France; https://orcid.org/0000-0002-5789-1292

Stéphanie Lerondel – TAAM imagerie in vivo, CNRS UAR44, 3B rue de la Férollerie, 45071 Orléans Cedex 2, France; https://orcid.org/0000-0002-4911-408X;

Laure Guénée – Laboratory of Crystallography, University of Geneva, Quai Ernest Ansermet 24, 1211 Geneva 4, Switzerland; orcid.org/0000-0002-2136-0510;

Céline Besnard – Laboratory of Crystallography, University of Geneva, Quai Ernest Ansermet 24, 1211 Geneva 4, Switzerland; orcid.org/0000-0001-5699-9675.

Author Contributions

The manuscript was written through contribution of all authors. All authors have given approval to the final version of the manuscript.

ACKNOWLEDGMENT

The results incorporated into this study have received funding from the Ligue Régionale Contre le Cancer (comités du Loiret et d'Eure-et-Loir, du Loir-et-Cher and de la Sarthe), the network "Molécules marines, métabolisme et cancer" from the Cancéropôle Grand Ouest, la Région Centre, the European Union's Horizon 2020 research and innovation programme under the Marie Skłodowska-Curie grant agreement No 665790 (G.C.). S.P. acknowledge support from the Institut National de la Santé et de la Recherche Médicale (Inserm). Authors are also grateful to Ms. Agnès Pallier for the help with ICP-AES measurements, to Dr. Mathieu Allix and to Mr. Emmanuel Véron for the help with powder X-ray diffraction experiments and to Mr. Rudy Clémençon for the 3D printing of the support of the phantom.

REFERENCES

1. Kenry; Duan, Y.; Liu, B., Recent Advances of Optical Imaging in the Second Near-Infrared Window. *Adv. Mater.* **2018,** *30*, 1802394.

2. Hong, G.; Antaris, A. L.; Dai, H., Near-infrared fluorophores for biomedical imaging. *Nat. Biomed. Eng.* **2017,** *1*, 0010.

3. Li, C.; Chen, G.; Zhang, Y.; Wu, F.; Wang, Q., Advanced Fluorescence Imaging Technology in the Near-Infrared-II Window for Biomedical Applications. *J. Am. Chem. Soc.* **2020,** *142*, 14789-14804.

4. Wang, L. V.; Hu, S., Photoacoustic Tomography: In Vivo Imaging from Organelles to Organs. *Science* **2012,** *335*, 1458-1462.

5. Steinberg, I.; Huland, D. M.; Vermesh, O.; Frostig, H. E.; Tummers, W. S.; Gambhir, S. S., Photoacoustic clinical imaging. *Photoacoustics* **2019,** *14*, 77-98.

6. Wang, L. V.; Yao, J., A practical guide to photoacoustic tomography in the life sciences. *Nat. Methods* **2016,** *13*, 627-638.

7. Attia, A. B. E.; Balasundaram, G.; Moothanchery, M.; Dinish, U. S.; Bi, R.; Ntziachristos, V.; Olivo, M., A review of clinical photoacoustic imaging: Current and future trends. *Photoacoustics* **2019,** *16*, 100144.

8. Wang, F.; Wan, H.; Ma, Z.; Zhong, Y.; Sun, Q.; Tian, Y.; Qu, L.; Du, H.; Zhang, M.; Li, L.; Ma, H.; Luo, J.; Liang, Y.; Li, W. J.; Hong, G.; Liu, L.; Dai, H., Light-sheet microscopy in the near-infrared II window. *Nat. Methods* **2019,** *16*, 545-552.

9. Karlas, A.; Pleitez, M. A.; Aguirre, J.; Ntziachristos, V., Optoacoustic imaging in endocrinology and metabolism. *Nat. Rev. Endocrinol.* **2021,** *17*, 323-335.

10. Beard, P., Biomedical photoacoustic imaging. *Interface Focus* **2011,** *1*, 602-631.

11. Karlas, A.; Fasoula, N.-A.; Paul-Yuan, K.; Reber, J.; Kallmayer, M.; Bozhko, D.; Seeger, M.; Eckstein, H.-H.; Wildgruber, M.; Ntziachristos, V., Cardiovascular optoacoustics: From mice to men – A review. *Photoacoustics* **2019,** *14*, 19-30.

12. Smith, A. M.; Mancini, M. C.; Nie, S., Bioimaging: second window for in vivo imaging. *Nat Nanotechnol* **2009,** *4*, 710-711.

13. Cheng, K.; Chen, H.; Jenkins, C. H.; Zhang, G.; Zhao, W.; Zhang, Z.; Han, F.; Fung, J.; Yang, M.; Jiang, Y.; Xing, L.; Cheng, Z., Synthesis, Characterization, and Biomedical Applications of a Targeted Dual-Modal Near-Infrared-II Fluorescence and Photoacoustic Imaging Nanoprobe. *ACS Nano* **2017,** *11*, 12276-12291.

14. Zlitni, A.; Gowrishankar, G.; Steinberg, I.; Haywood, T.; Sam Gambhir, S., Maltotriose-based probes for fluorescence and photoacoustic imaging of bacterial infections. *Nat. Commun.* **2020,** *11*, 1250.

15. Bhattacharyya, S.; Wang, S.; Reinecke, D.; Kiser, W., Jr.; Kruger, R. A.; DeGrado, T. R., Synthesis and evaluation of near-infrared (NIR) dye-herceptin conjugates as photoacoustic computed tomography (PCT) probes for HER2 expression in breast cancer. *Bioconjugate chemistry* **2008,** *19* (6), 1186-93.

16. Swierczewska, M.; Choi, K. Y.; Mertz, E. L.; Huang, X.; Zhang, F.; Zhu, L.; Yoon, H. Y.; Park, J. H.; Bhirde, A.; Lee, S.; Chen, X., A Facile, One-Step Nanocarbon Functionalization for Biomedical Applications. *Nano Lett.* **2012,** *12* (7), 3613-3620.

17. Huynh, E.; Leung, B. Y. C.; Helfield, B. L.; Shakiba, M.; Gandier, J.-A.; Jin, C. S.; Master, E. R.; Wilson, B. C.; Goertz, D. E.; Zheng, G., In situ conversion of porphyrin microbubbles to nanoparticles for multimodality imaging. *Nat. Nanotechnol.* **2015,** *10*, 325-332.

18. Lovell, J. F.; Jin, C. S.; Huynh, E.; Jin, H.; Kim, C.; Rubinstein, J. L.; Chan, W. C. W.; Cao, W.; Wang, L. V.; Zheng, G., Porphysome nanovesicles generated by porphyrin bilayers for use as multimodal biophotonic contrast agents. *Nat. Mater.* **2011,** *10*, 324-332.

19. Zhang, X.; Wu, Y.; Chen, L.; Song, J.; Yang, H., Optical and Photoacoustic Imaging In Vivo: Opportunities and Challenges. *Chem. Biomed. Imag.* **2023,** *1* (2), 99-109.

20. Martinić, I.; Eliseeva, S. V.; Petoud, S., Near-infrared emitting probes for biological imaging: Organic fluorophores, quantum dots, fluorescent proteins, lanthanide(III) complexes and nanomaterials. *J. Lumin.* **2017,** *189*, 19-43.

21. Ning, Y. Y.; Zhu, M. L.; Zhang, J. L., Near-infrared (NIR) lanthanide molecular probes for bioimaging and biosensing. *Coord. Chem. Rev.* **2019,** *399*, 213028.

22. Xu, J.; Gulzar, A.; Yang, P.; Bi, H.; Yang, D.; Gai, S.; He, F.; Lin, J.; Xing, B.; Jin, D., Recent advances in near-infrared emitting lanthanide-doped nanoconstructs: Mechanism, design and application for bioimaging. *Coord. Chem. Rev.* **2019,** *381*, 104-134.

23. Bünzli, J.-C. G.; Eliseeva, S. V., Photophysics of Lanthanoid Coordination Compounds. In *Comprehensive Inorganic Chemistry II*, Yam, V. W.-W., Ed. Elsevier B.V.: Amsterdam, 2013; Vol. 8, pp 339-398.

24. Eliseeva, S. V.; Bünzli, J.-C. G., Lanthanide luminescence for functional materials and bio-sciences. *Chem. Soc. Rev.* **2010,** *39*, 189-227.

25. Bünzli, J.-C. G., Lanthanide Luminescence for Biomedical Analyses and Imaging. *Chem. Rev.* **2010,** *110*, 2729-2755.

26. Weissman, S. I., Intramolecular Energy Transfer The Fluorescence of Complexes of Europium. *J. Chem. Phys.* **1942,** *10*, 214-217.

27. Bünzli, J.-C. G.; Eliseeva, S. V., Basics of Lanthanide Photophysics. In *Lanthanide Luminescence: Photophysical, Analytical and Biological Aspects*, Hänninen, P.; Härmä, H., Eds. Springer Berlin Heidelberg: Berlin, Heidelberg, 2011; pp 1-45.

28. Sato, S.; Wada, M., Relations between Intramolecular Energy Transfer Efficiencies and Triplet State Energies in Rare Earth β-diketonates. *Bull. Chem. Soc. Jpn.* **1970,** *43*, 1955-1962.

29. Binnemans, K., Chapter 225 - Rare-earth beta-diketonates. In *Handbook on the Physics and Chemistry of Rare Earths*, Gschneidner, K. A.; Bünzli, J.-C. G.; Pecharsky, V. K., Eds. Elsevier: 2005; Vol. 35, pp 107-272.

30. Wang, H.; Qian, G.; Wang, M.; Zhang, J.; Luo, Y., Enhanced Luminescence of an Erbium (III) Ion-Association Ternary Complex with a Near-Infrared Dye. *J. Phys. Chem. B* **2004,** *108*, 8084-8088.

31. Wang, H.; Yang, Y.; Cui, Y.; Wang, Z.; Qian, G., Sensitized near-infrared luminescence from erbium ion-associated complex with IR140 dye. *Dyes Pigm.* **2012,** *95*, 69-73.

32. Xu, H.-B.; Chen, X.-L.; Deng, J.-G.; Deng, Z.-H.; Huang, S.-L.; Kurmoo, M.; Zeng, M.-H., Sensitized near infrared emission through supramolecular d → f energy transfer within an ionic Ru(II)–Er(III) pair. *Dalton Trans.* **2018,** *47*, 2073-2078.

33. Peng, Y.; Ye, H.; Li, Z.; Motevalli, M.; Hernández, I.; Gillin, W. P.; Wyatt, P. B., Visible-Range Sensitization of Er^{3+}-Based Infrared Emission from Perfluorinated 2-Acylphenoxide Complexes. *J. Phys. Chem. Lett.* **2014,** *5*, 1560-1563.

34. Liu, C.; Eliseeva, S. V.; Luo, T.-Y.; Muldoon, P. F.; Petoud, S.; Rosi, N. L., Near infrared excitation and emission in rare earth MOFs via encapsulation of organic dyes. *Chem. Sci.* **2018,** *9*, 8099-8102.

35. Comby, S.; Bünzli, J.-C. G., Lanthanide Near-Infrared Luminescence in Molecular Probes and Devices. In *Handbook on the Physics and Chemistry of Rare Earths*, Gschneidner Jr., K. A.; Bünzli, J.-C. G.; Pecharsky, V. K., Eds. Elsevier Science B.V.: Amsterdam, 2007; Vol. 37, Ch. 235, pp 217-470.

36. Ning, Y.; Chen, S.; Chen, H.; Wang, J.-X.; He, S.; Liu, Y.-W.; Cheng, Z.; Zhang, J.-L., A proof-of-concept application of water-soluble ytterbium(iii) molecular probes in in vivo NIR-II whole body bioimaging. *Inorg. Chem. Front.* **2019,** *6* (8), 1962-1967.

37. Wang, T.; Wang, S.; Liu, Z.; He, Z.; Yu, P.; Zhao, M.; Zhang, H.; Lu, L.; Wang, Z.; Wang, Z.; Zhang, W.; Fan, Y.; Sun, C.; Zhao, D.; Liu, W.; Bünzli, J.-C. G.; Zhang, F., A hybrid erbium(III)–bacteriochlorin near-infrared probe for multiplexed biomedical imaging. *Nat. Mater.* **2021,** *20*, 1571-1578.

38. Melby, L. R.; Rose, N. J.; Abramson, E.; Caris, J. C., Synthesis and Fluorescence of Some Trivalent Lanthanide Complexes. *J. Am. Chem. Soc.* **1964,** *86* (23), 5117-5125.

39. Sager, W. F.; Filipescu, N.; Serafin, F. A., Substituent Effects on Intramolecular Energy Transfer. I. Absorption and Phosphorescence Spectra odf Rare Earth .b.- Diketonates. *J. Phys. Chem.* **1965,** *69*, 1092-1100.

40. Benson, R. C.; Kues, H. A., Absorption and fluorescence properties of cyanine dyes. *J. Chem. Eng. Data* **1977,** *22*, 379-383.

41. Beeby, A.; Clarkson, I. M.; Dickins, R. S.; Faulkner, S.; Parker, D.; Royle, L.; de Sousa, A. S.; Williams, J. A. G.; Woods, M., Non-radiative deactivation of the excited states of europium, terbium and ytterbium complexes by proximate energy-matched OH, NH and CH oscillators: an improved luminescence method for establishing solution hydration states. *J. Chem. Soc. Perkin Trans. 2* **1999**, 493-503.

42. Martinić, I.; Eliseeva, S. V.; Collet, G.; Luo, T.-Y.; Rosi, N.; Petoud, S., One Approach for Two: Toward the Creation of Near-Infrared Imaging Agents and Rapid Screening of Lanthanide(III) Ion Sensitizers Using Polystyrene Nanobeads. *ACS Appl. Bio Mater.* **2019,** *2*, 1667-1675.

43. Toth, E.; Lacerda, S.; Delalande, A.; Eliseeva, S. V.; Pallier, A.; Bonnet, C. S.; Szeremeta, F.; Même, S.; Pichon, C.; Petoud, S., Dox-

orubicin-sensitized Luminescence of NIR-emitting Ytterbium Liposomes: Towards Direct Monitoring of Drug Release. *Angew. Chem. Int. Ed.* **2021,** *60*, 23574-23577.

44. Arconada-Alvarez, S. J.; Lemaster, J. E.; Wang, J.; Jokerst, J. V., The development and characterization of a novel yet simple 3D printed tool to facilitate phantom imaging of photoacoustic contrast agents. *Photoacoustics* **2017,** *5*, 17-24.

45. Pu, K.; Shuhendler, A. J.; Jokerst, J. V.; Mei, J.; Gambhir, S. S.; Bao, Z.; Rao, J., Semiconducting polymer nanoparticles as photoacoustic molecular imaging probes in living mice. *Nat. Nanotechnol.* **2014,** *9*, 233-239.

46. Wang, H.; Liu, C.; Gong, X.; Hu, D.; Lin, R.; Sheng, Z.; Zheng, C.; Yan, M.; Chen, J.; Cai, L.; Song, L., In vivo photoacoustic molecular imaging of breast carcinoma with folate receptor-targeted indocyanine green nanoprobes. *Nanoscale* **2014,** *6*, 14270-14279.

47. Weber, J.; Beard, P. C.; Bohndiek, S. E., Contrast agents for molecular photoacoustic imaging. *Nat. Methods* **2016,** *13*, 639-650.

48. Balasundaram, G.; Ho, C. J. H.; Li, K.; Driessen, W.; Dinish, U. S.; Wong, C. L.; Ntziachristos, V.; Liu, B.; Olivo, M., Molecular photoacoustic imaging of breast cancer using an actively targeted conjugated polymer. *Int. J. Nanomed.* **2015,** *10*, 387-397.

49. Upputuri, P. K.; Pramanik, M., Recent advances in photoacoustic contrast agents for in vivo imaging. *Wiley Interdiscip. Rev. Nanomed. Nanobiotechnol.* **2020,** *12*, e1618.

For Table of Contents